Critical role of CD206+ macrophages in organizing anti-tumor immunity

Arja Ray[1,2], Kenneth H. Hu[1,2,#], Kelly Kersten[1,2], Nicholas F. Kuhn[1,2], Bushra Samad[2,3], Alexis J. Combes[1,2,3,4], Matthew F. Krummel[1,2,3*]

Affiliations:
[1]Department of Pathology, [2]ImmunoX Initiative, [3]UCSF CoLabs, [4]Department of Medicine, University of California, San Francisco, CA 94143, USA. [#]Current Address: Department of Immunology, The University of Texas MD Anderson Cancer Center and James P Allison Institute

***Corresponding Author:**
Matthew F. Krummel, Ph.D.
513 Parnassus Avenue, HSW 512
San Francisco, CA 94143-0511
matthew.krummel@ucsf.edu
Tel: (415) 514-3130
Fax: (415) 514-3165

Abstract:

Tumor-associated macrophages (TAMs) are frequently and simplistically categorized as immunosuppressive, and one molecule prominently used to highlight their so-called 'M2' state is the surface protein CD206. However, direct evidence of the impact of macrophages remains impaired by the lack of sufficiently penetrant and specific tools to manipulate them in vivo. We thus made a novel conditional CD206 knock-in mouse to specifically visualize and/or deplete these TAMs. Early depletion of CD206+ macrophages and monocytes (here, 'MonoMacs') strikingly led to an indirect loss of a key anti-tumor network of NK cells, conventional type I dendritic cells (cDC1) and CD8 T cells. Among myeloid cells, we found that the CD206+ TAMs are the primary producers of CXCL9, the well-established chemoattractant for CXCR3-expressing NK and CD8 T cells. In contrast, a population of stress-responsive TAMs ("Hypoxic" or *Spp1*+) and immature monocytes, which remain following depletion, expressed vastly diminished levels of CXCL9. We confirmed that the missing NK and CD8 T cells are the primary producers of the cDC1-attracting chemokine *Xcl1* and cDC1 growth factor *Flt3l*. Consistent with the loss of this critical network, CD206+ TAM depletion decreased tumor control in mice. Likewise, in humans, the CD206+ MonoMac signature correlated robustly with stimulatory cDC1 signature genes. Together, these findings negate the classification of CD206+ macrophages as immunosuppressive and instead illuminate the role of this majority of TAMs in organizing a critical tumor-reactive archetype of immunity.

Introduction:

Macrophages have diverse roles in homeostasis and disease and a refined understanding of their impact on anti-tumor immunity is an imperative, given the current impetus in developing myeloid targeting therapies for cancer(*1, 2*). A widely used shortcut for describing macrophages involves an 'M1' versus 'M2' nomenclature, derived from in vitro skewing with Th1 versus Th2 cytokines, and often equated with pro and anti-inflammatory functions respectively. However, this binary M1/M2 delineation of macrophage phenotype does not capture the heterogeneity at the single cell level (*3-5*). In addition, there is scant evidence of these markers being part of coordinated gene programs in vivo. In wound healing, *Arg1* and *Mrc1*(gene corresponding to the mannose-binding C-type lectin CD206), both purportedly key markers of an M2 state, have entirely distinct expression patterns (*6*). In both mouse and human tumors, there is also a complete lack of correlation among genes characterizing M1 or M2 phenotypes within MonoMacs (*3*). In fact, M1 and M2 signatures in MonoMacs often show correlated instead of opposing expression patterns in tumors (*4, 5*). Nonetheless, myeloid cells expressing CD206, sometimes therefore designated as 'M2-like', continue to be used as a marker of a state equated with immunosuppression. The detrimental effects of tumor-associated macrophages (TAMs) on anti-tumor immunity have indeed been highlighted by a number of critical studies (*7-11*). However, a holistic dissection of the role of CD206-expressing MonoMacs in tumors in vivo is lacking and the nomenclature thus persists. We therefore developed a conditional knock-in reporter mouse using the *Mrc1* (CD206) allele that allows specific visualization and depletion of those cells to define their true impact on anti-tumor immunity.

Results:

To highlight CD206 surface expression variation across MonoMac differentiation in tumors, we identified relevant subsets from single cell transcriptomics in B16F10 tumors (**Fig. 1A**, (*3*)), and

applied flow cytometry to enrich for the indicated populations in a related B78chOVA ((*11*); B78: an amelanotic clone of B16, chOVA: mCherry and Ovalbumin) tumor model. CD206 was most prominently expressed by terminal VCAM-1^{hi}IL-7Rα^{lo} C1q TAMs followed by the VCAM-1^{lo}IL-7Rα^{hi} stress populations (associated with enriched glycolysis, increased *Spp1* expression(*3, 12*) and possibly hypoxia(*13*)). In contrast, CD206 was expressed at low levels by other less differentiated VCAM^{-}IL-7Ra^{-} (DN) TAMs (**Fig. 1B, C**). Among monocytes, the MHCII+ subset was the prominent CD206 expressor as opposed to early (immature, MHCII-) monocytes, albeit at lower levels than Stress and C1q TAMs (**Fig. 1B, C**). Overall, this analysis showed that CD206 is variably expressed across all monocyte and macrophage subsets, and generally increases with differentiation. However, when considering the use of this protein and the gene encoding it as a means of eliminating these macrophages and thereby studying their function, we noted that this scavenger receptor is frequently also expressed on other cells including endothelial cells and keratinocytes (*14, 15*) and may further be ectopically produced by other cells in the TME.

We thus generate a conditional system where a lineage-specific Cre could drive the recombination of a 3' knock-in *Mrc1*$^{LSL\text{-}Venus\text{-}DTR}$ allele (Venus : Yellow Fluorescent Protein variant for visualization; DTR: Diphtheria toxin receptor for depletion) (**Fig. 1D**). Then, using a *Csf1r*^{Cre}; *Mrc1*$^{LSL\text{-}Venus\text{-}DTR}$ cross (DTR), compared to a *Mrc1*$^{LSL\text{-}Venus\text{-}DTR}$ (WT) control, we assessed the reporter expression in various immune and CD45- non-immune compartments in the subcutaneous melanoma model B78chOVA (**Fig. 1D, Supplementary Fig. S1A**). As predicted from CD206 expression, nearly 75% of TAMs showed profound Venus expression tightly correlated with surface expression of CD206 protein (**Fig. 1F**). We also found that nearly half of cDC2s, consistent with their monocytic origin as previously described(*16*), expressed Venus in this system. A small subset of CD206+ monocytes expressed the reporter, again consistent with *Csf1r* driven expression. Weak expression was also found in a yet smaller population of

neutrophils. When viewed by the level of CD206-driven expression of the Venus marker, macrophages were 2-3x brighter than the other populations (**Fig. 1F**). Importantly, no reporter expression was detected in non-immune cells, lymphocytes and cDC1s (**Fig. 1E, F**). Likewise, in the proximal tumor-draining lymph node (tdLN), the same hierarchy of expression patterns was observed, albeit at much lower levels (**Supplementary Fig. S1B**). In addition, some tissue-resident macrophages, such as alveolar macrophages in the lung express high levels of CD206 and therefore the reporter, while interstitial macrophages, monocytes, neutrophils, and non-immune cells again showed very modest to no expression (**Supplementary Fig. S2**). Therefore, in *Csf1r*^{Cre}; *Mrc1*$^{LSL\text{-}Venus\text{-}DTR}$ mice, a robust marking of mature CD206+ macrophages in the tumor was observed, along with faithful marking of CD206+ subsets of monocytes, neutrophils and cDC2s, but not cDC1s, lymphocytes and non-immune cells.

CD206+ TAM depletion leads to indirect loss of a reactive immune archetype: To test the impact of CD206+ macrophages on the overall tumor immune microenvironment, we took advantage of the linkage of Venus and DTR expression in this background to deplete those cells. We first confirmed that Cre-mediated induction of reporter expression without diphtheria toxin (DTx) administration did not alter the immune composition of subcutaneous B78chOVA tumors with adoptively transferred antigen-specific OT-I cells in the WT vs. DTR mice (**Supplementary Fig. S3**). With this baseline, we administered DTx either 'late/acute', namely in the last 4 days prior to the tumor harvest or 'early/chronic', i.e., every day 2-3 days, starting 2 days post T cell injection until harvest to parse out the role of CD206+ MonoMacs in the TME.

In the context of late DTx administration, we confirmed that this regimen specifically depleted the cells of interest and otherwise had little effect on other non-targeted cells. Thus, there was a strong reduction in the TAMs (**Figure 2B**) which corresponded to a specific loss of the CD206+ populations (**Fig. 2P**). We found a compensatory rise in monocytes overall, accompanied by a

specific loss of its CD206+ subset (**Figure 2C, 2P**). No significant loss was observed in cDC2s, cDC1s, NK cells, the adoptively transferred OTI, or neutrophils (**2D-H**), although the regimen did select against the CD206+ populations in each case (**Figure 2P**). Thus, direct depletion was reliably restricted to the highest expressors of the construct, namely the CD206+ TAM and monocyte populations.

When we depleted CD206+ populations with DTx early, i.e., starting 2d after OTI adoption, again we found robust depletion of TAMs (**Fig. 2I**) expectedly with a strong selection against those expressing CD206 (**Fig. 2Q**). As before, the CD206+ subsets of other populations were still depleted—robustly in monocytes and cDC2s and mildly in neutrophils (**Fig. 2Q**). A compensatory increase in neutrophils was observed, while overall abundance of monocytes, albeit biased towards CD206-, remained similar, in contrast to acute depletion. (**Fig. 2J, L**). Strikingly, under this early elimination regime, we also observed a profound decrease in intratumoral CD103+ cDC1 abundance (**Fig. 2M**). Further NK cells and transferred OT-I abundance in the tumor was also significantly compromised (**Fig. 2N, O**). Noting that none of these CD8, NK and cDC1 populations express the reporter, we concluded that a direct, targeted ablation of 'M2-like' CD206+ MonoMacs led to a unique disruption of the tumor immune microenvironment and the indirect loss of this key anti-tumor reactive archetype comprising of NK cells, cDC1s and antigen specific CD8 T cells(*17*) (**Fig. 2R**).

These trends in abundances were similar when expressed as percentage of live cells in all cases except the increase in monocytes following acute depletion (**Supplementary Fig. S4**), which only trended higher. Further, when we similarly treated non-tumor bearing DTR mice with DTx with six doses akin to the early depletion regimen in tumors, and analyzed the immune compositions in the skin (site of the ectopic tumor injections) and skin draining lymph nodes (**Supplementary Fig. S5A**), no robust indirect loss of populations were observed. We found instead a modest uptick in

147 monocyte abundance, a minor reduction in CD8 T cells in the skin draining lymph node
148 (**Supplementary Fig. S5B-G**), and an increase of neutrophils in an otherwise scarcely immune-
149 populated skin (**Supplementary Fig. S5H-M**). Notably, the expected CD206+ subsets of myeloid
150 cells were again reliably depleted both in the skin and skin draining LNs (**Supplementary Fig.**
151 **S5N, O**). Therefore, early depletion in tumors specifically produced the robust indirect loss of the
152 cDC1:NK:CD8 module, suggesting that CD206+ MonoMacs were involved in the recruitment and
153 early establishment of this reactive archetype in the TME.
154
155 **CD206+ MonoMacs are enriched in CXCL9 and associated with *Cxcr3*-expressing**
156 **lymphocytes:** To spatially map the CD206+ MonoMac population in tumors, we used two-photon
157 microscopy of B78chOVA tumor slices to visualize the localization of reporter-expressing
158 macrophages and transferred OT-I T cells marked by the CD2dsRed allele (**Fig. 3A**). Doing this
159 revealed three distinct niches of CD206+ macrophage and T cell localization– edge: macrophage
160 and collagen-rich with modest T cell presence, mid: the interfacial layer with abundant T cell:
161 macrophage interaction zones and interior: bulk of the tumor sparser in both immune cell types
162 (**Fig. 3A**). To define the macrophage subtypes associated with reactive immunity and their
163 potential spatially segregated modes of action, we performed post-imaging spatial transcriptomics
164 by ZipSeq (*18*) on CD45+ cells in these three zones (*11*) with or without early DTx treatment
165 harvested at d12 post T cell injection. UMAP projection of non-linear dimensional reduction and
166 louvain clustering clearly showed the remarkable shift in tumor immune composition among
167 control and DTx treated groups (**Fig. 3B, C, Supplementary Fig. S6A**). Notably, previously-
168 defined C1q and Stress-responsive (Stress) TAMs, which most robustly express CD206 at the
169 protein level, along with MHCII+ and Interferon-stimulatory gene (ISG) -expressing monocytes
170 were expectedly depleted by direct DTx action (**Fig. 3C, Supplementary Fig. S6A**). On the other
171 hand, early monocytes, neutrophils and a *Spp1*, *Hif1*α-expressing subset related to the Stress
172 TAMs by shared expression of *Arg1, Il7r* (i.e., Stress^{Spp1} TAM), became prominent in their place

(**Fig. 3C, Supplementary Fig. S6A**). The loss of cDC1:NK:CD8 populations was again robustly evident in the analysis of relative abundance from the scRNASeq data (**Fig. 3C**). Here, the changes in immune subpopulations were not localized to a specific region of the tumor (**Fig. 3C**) but permeated throughout as a holistic overhaul of the tumor immune microenvironment.

Given that a well-established positive functional role of TAMs is the production of CXCL9 and CXCL10, inducing CXCR3-dependent lymphocyte recruitment in tumors(*19*), we sought to understand the relationship between CD206 positive myeloid populations and this axis. Analyzing RNAseq data in detail, we found that expression of *Cxcl9* in particular was dramatically reduced in the DTx treated tumors (**Fig. 3D, Supplementary Fig. S6B**), and this corresponded to substantial expression by the directly depleted subsets (CD206+MHCII+ MonoMacs) and none of the indirectly increased ones (Early Mono, Stress^{Spp1} TAM and Neutrophils) (**Fig. 3E, Supplementary Fig. S6C**). We then undertook flow cytometry for intracellular CXCL9 expression which revealed a positively association between this and CD206 expression in TAMs (**Fig. 3F**). Since CD206-depleted tumors still had small numbers of lymphocytes, we compared their levels of the ligand for these cytokines and found that *Cxcr3* expression was largely absent in the DTx treated condition in all the lymphocytes, as opposed to a robust expression in the control group (**Fig. 3G, Supplementary Fig. S6D**).

Lymphocytes are also key producers of cDC1-formative chemokines FLT3L (*17*) and XCL1(*20*) and given the loss of cDC1s in concert with lymphocytes with this depletion regime, we probed for these chemokines in the remnant lymphocytes in control vs. CD206-depleted dataset. This demonstrated that both *Flt3l* (**Fig. 3H, Supplementary Fig. S6F**) and *Xcl1* (**Fig. 3I, Supplementary Fig. S6E**) were absent in the NK cells and CD8 T cells in the DTx-treated condition. These data are consistent with CXCL9-expressing CD206+ MonoMacs lying at the

198 center of the organization of reactive anti-tumor immunity comprising of CXCL9-reponsive NK,
199 CD8 T cells and cDC1s.
200
201 **CD206+ TAMs are required for CD8 T cell mediated anti-tumor immunity:** Given the
202 widespread contention that 'M2' macrophages defined by CD206 expression were especially
203 inhibitory for tumor immunity, we asked whether they were necessary for successful CD8 T cell
204 mediated tumor regression. To test this, we used a MC38chOVA model and an adoptive transfer
205 of OT-I T cells that results in efficient tumor control(*21*). We confirmed first that reporter expression
206 in these tumors followed largely the same pattern as the B78chOVA tumors, with substantial
207 expression only in TAMs and cDC2s, albeit at lower levels due to the overall lower CD206+
208 fraction, and little to no expression in neutrophils and monocytes in this model. (**Supplementary**
209 **Fig. S7A, B**). Importantly and as previously, lymphocytes and cDC1s showed no reporter
210 expression (**Supplementary Fig. S7A, B**). As with the B78chOVA model, we applied early and
211 late depletion regimens to the MC38chOVA tumors, first without the addition of OT-I T cells, to
212 assess differential effects on early establishment and maintenance of immune cells without the
213 confounding variable of tumor regression (**Fig. 4A**). We first confirmed that following reporter
214 expression patterns, the CD206+ subsets were depleted robustly in TAMs and cDC2s and
215 modestly in monocytes and neutrophils in both the late (**Fig. 4I**) and early (**Fig. 4J**) depletion
216 regimens. Some differences were observed compared to the B78chOVA model, including an
217 overall maintenance of TAM abundance in late depletion (**Supplementary Fig. S8B, F**) despite
218 depletion of the CD206+ populations (**Fig. 4B, E**). We also noted slight variations namely
219 increased monocyte infiltration in early but not late depletion (**Supplementary Fig. S8C, G**),
220 neutrophil enrichment in both regimens (**Supplementary Fig. S8E, I**). As in the case of
221 B78chOVA tumors, CD206+ cDC2s were depleted (**Fig. 4I, J**) but no change was detected in
222 overall cDC2 abundance (**Supplementary Fig. S8D, H**), presumably representing selection

against the CD206+ fraction. Importantly, there was once again a robust indirect loss of cDC1s and lymphocytes specifically under the early but not the late depletion regimen (**Fig. 4C, D, F, G**).

With confirmation of this key indirect effect of CD206+ TAM depletion in the MC38chOVA model, we treated subcutaneous MC38chOVA tumors in WT and DTR mice with OT-Is with concomitant early DTx administration (**Fig. 4H**) and tracked changes in tumor size. This demonstrated significantly reduced OT-I-mediated tumor control of MC38chOVA tumors (**Fig. 4H**) in the DTR group -i.e., when CD206+ TAMs were depleted.

While these data provided substantial evidence that CD206+ populations of monocytes and macrophages were in fact positive contributors to reactive anti-tumor immunity in mice, we sought to determine whether the revealed relationships of our study also extended to human disease. To do so, we first applied differential gene expression (DGE) analysis of the Ctrl vs. DTx treated MonoMac populations from our scRNASeq dataset (**Fig. 3B**) and obtained the human orthologs for the top 10 enriched genes in each group. We then used these genes to create signatures for $CD206^{hi}$ (top 10 enriched in Ctrl) and $CD206^{lo}$ (top 10 enriched in DTx treated) MonoMac populations (**Fig. 4K**). As expected, the former not only included *CXCL9, C1QA, APOE* but also several MHC-II related genes, while the latter included *IL1B* and other chemokines such as *CXCL2* and *CXCL3* along with *SPP1* which we've associated with the 'stress' and 'hypoxia' (Hif1a-positive, glycolytic) population. We took advantage of a unique myeloid-specific bulk RNA-Seq data from a curated dataset of sorted myeloid, T cell and live cells from >250 human tumor biopsies(*22*). Using the two signatures, we found that the $CD206^{hi}$ but not the $CD206^{lo}$ MonoMac signature correlated significantly with the tumor-reactive stimulatory cDC1s (stimulatory dendritic cell or SDC) signature (**Fig. 4L, M**)(*10*). Given that it is by now well-established that SDCs are critical for anti-tumor immunity and checkpoint blockade responsiveness(*17, 20*), we also queried whether the relative abundance of CD206+ macrophages (i.e., $CD206^{hi}/CD206^{lo}$ ratio) was

correlated with better survival in patients. We again applied these gene signatures ($CD206^{hi}$/$CD206^{lo}$) taken specifically from the myeloid cells for each patient in a cohort of >230 patients from the most common indications in the dataset (which are CRC: Colorectal Cancer, GYN: Gynecological Cancer, HNSC: Head and Neck Squamous Cell Carcinoma, KID: Kidney Cancer; LUNG: Lung Carcinoma). We then stratified patients into the top and bottom 40% with respect to this ratio of $CD206^{hi}$: $CD206^{lo}$ gene signatures and queried patient outcomes against this metric. This indicator of relative skewing towards $CD206^{hi}$ MonoMacs was a robust predictor of favorable survival outcomes in human patients (**Fig. 4N**). Therefore, contrary to the paradigm of CD206 expressing macrophages as immunosuppressive, this data shows that $CD206^{hi}$, as opposed to $CD206^{lo}$ MonoMacs are a critical organizing fulcrum for the reactive archetype of NK cells, cDC1s and CD8 T cells. Taken together, these data establish a nuanced understanding of the context-dependent role of TAMs in the TME that is necessary to rationally design next-generation myeloid-targeting immunotherapies in cancer.

Discussion: cDC1s have been previously linked to FLT3L and XCL1 producing NK cells and activated CD8 T cells. These same lymphocytes in turn may be recruited and expanded by chemokines and antigen-presentation by cDC1s, creating a virtuous feedback loop for anti-tumor immunity(*10, 17, 20*). It was, however, previously unexplored how specific macrophage subsets support or thwart this strong anti-tumor archetype. Here, we demonstrate that CD206+ macrophages both robustly express CXCL9 and play a critical role in initiating the assembly of an anti-tumor reactive archetype of cDC1s, NK cells and CD8 T cells in tumors.

Previous work had already indicated that an M1/M2 dichotomy of macrophage phenotypes is nebulous in the transcriptomic space as no genes associated with ‘M1-ness’ correlates either positively with other purported ‘M1’ genes nor inversely with ’M2’ genes, and the same is found

for 'M2' genes (*3, 5*). Nevertheless, macrophages bearing CD206 continue to be a purported category of simplistic characterization as immunosuppressive and 'M2-like'. Here, we definitively shows that distinction to be incorrect. Rather, they are important for overall recruitment of inflammatory cells and the very marker—CD206—which is often associated with immunosuppression in fact correlates very highly with the inflammatory chemokine CXCL9. In this context, recent data on using *CXCL9* and *SPP1* gene expression to functionally classify macrophages in human tumors (*12*) are aligned with our findings and provide further support to this biology we have uncovered here, albeit without direct focus on CD206. Notably, in our previous work on MonoMac differentiation(*3*), the *SPP1*-expressing Stress^{Spp1} TAMs were observed robustly in human tumors and were likely embedded within the Arg1 TAM subset in mice, and only emerge as a distinct cluster here due to their disproportionate enrichment post depletion. As we've previously noted(*3*), these non-CD206 expressing 'Stress' macrophages are distinctly glycolytic, express *Hif1a*, and are likely the cells that have previously been defined as 'hypoxic' macrophages.

The robust association between CD206+ macrophages depletion and specific loss of *Cxcr3*+ lymphocytes suggests that it is the loss of CXCR3-dependent lymphocyte recruitment (*19*) which is the primary driver leading to the loss of the key tumor-reactive archetype. However, the indirect effects of changes in the TME, especially the specific origin and role of the proportionally expanded neutrophil frequency remains undetermined. Indeed, previous studies have reported variable responses in terms of compensatory neutrophil influx when depleting cells of monocytic origin in tumors(*23-25*). One interpretation of the lack of a similarly robust expansion in the late depletion regime suggests that a microenvironment-dependent opportunistic filling of the early myeloid niche by neutrophils may take place in the absence of sufficient MonoMacs and the reactive immune components.

As such, many questions regarding the specific role of TAMs have remained obscured or unanswered partly owing to the lack of sufficiently specific and penetrant tools to manipulate them in vivo. Commonly used methods, while useful lack sufficient specificity, include the depletion of all monocytes and monocyte-derived dendritic cells (CSF1R blocking antibody;(*26*-*28*)) and the depletion of all phagocytic cells and arrest of neutrophils (Clodronate; (*29*)). In this context, the novel CD206 reporter introduced here provides a more selective marking and depletion tool for CD206+ TAMs, with a further potential to target various subpopulations of by altering the Cre driver alleles. Our results indicate that total or even 'M2-specific' depletion of MonoMac populations may not be prudent and provides a basis to further refine strategies of targeting. To this extent, while anti-CSF1R antibodies have failed to show benefits in clinical trials (*30*), other strategies using for example, antibodies that trigger TREM1 (which is specifically expressed by the myeloid cells that become prominent with CD206+ MonoMac depletion) and subsequent changes in those macrophages may prove more surgical(*31*). Systematically dissecting the role of individual TAM subtypes will be crucial to deciphering their context-dependent and complex roles in the TME, with a view towards harnessing them for better immunotherapy outcomes.

References:

1. M. Binnewies *et al.*, Understanding the tumor immune microenvironment (TIME) for effective therapy. *Nat Med* **24**, 541-550 (2018).
2. S. Goswami, S. Anandhan, D. Raychaudhuri, P. Sharma, Myeloid cell-targeted therapies for solid tumours. *Nat Rev Immunol* **23**, 106-120 (2023).
3. A. M. Mujal *et al.*, Holistic Characterization of Tumor Monocyte-to-Macrophage Differentiation Integrates Distinct Immune Phenotypes in Kidney Cancer. *Cancer immunology research* **10**, 403-419 (2022).
4. S. Cheng *et al.*, A pan-cancer single-cell transcriptional atlas of tumor infiltrating myeloid cells. *Cell* **184**, 792-809 e723 (2021).
5. E. Azizi *et al.*, Single-Cell Map of Diverse Immune Phenotypes in the Breast Tumor Microenvironment. *Cell* **174**, 1293-1308 e1236 (2018).
6. K. H. Hu *et al.*, Transcriptional space-time mapping identifies concerted immune and stromal cell patterns and gene programs in wound healing and cancer. *Cell Stem Cell* **30**, 885-903 e810 (2023).
7. A. L. Doedens *et al.*, Macrophage expression of hypoxia-inducible factor-1 alpha suppresses T-cell function and promotes tumor progression. *Cancer Res* **70**, 7465-7475 (2010).
8. B. Ruffell *et al.*, Macrophage IL-10 blocks CD8+ T cell-dependent responses to chemotherapy by suppressing IL-12 expression in intratumoral dendritic cells. *Cancer Cell* **26**, 623-637 (2014).
9. E. Peranzoni *et al.*, Macrophages impede CD8 T cells from reaching tumor cells and limit the efficacy of anti-PD-1 treatment. *Proc Natl Acad Sci U S A* **115**, E4041-E4050 (2018).
10. M. L. Broz *et al.*, Dissecting the Tumor Myeloid Compartment Reveals Rare Activating Antigen-Presenting Cells Critical for T Cell Immunity. *Cancer Cell* **26**, 938 (2014).
11. K. Kersten *et al.*, Spatiotemporal co-dependency between macrophages and exhausted CD8+ T cells in cancer. *Cancer Cell* **40**, 624-638.e629 (2022).
12. R. Bill *et al.*, CXCL9:SPP1 macrophage polarity identifies a network of cellular programs that control human cancers. *Science* **381**, 515-524 (2023).
13. J. Wei *et al.*, Characterizing Intercellular Communication of Pan-Cancer Reveals SPP1+ Tumor-Associated Macrophage Expanded in Hypoxia and Promoting Cancer Malignancy Through Single-Cell RNA-Seq Data. *Front Cell Dev Biol* **9**, 749210 (2021).
14. J. T. Chi *et al.*, Endothelial cell diversity revealed by global expression profiling. *Proc Natl Acad Sci U S A* **100**, 10623-10628 (2003).
15. G. Szolnoky *et al.*, A mannose-binding receptor is expressed on human keratinocytes and mediates killing of Candida albicans. *J Invest Dermatol* **117**, 205-213 (2001).
16. Z. Liu *et al.*, Dendritic cell type 3 arises from Ly6C(+) monocyte-dendritic cell progenitors. *Immunity* **56**, 1761-1777 e1766 (2023).
17. K. C. Barry *et al.*, A natural killer-dendritic cell axis defines checkpoint therapy-responsive tumor microenvironments. *Nat Med* **24**, 1178-1191 (2018).
18. K. H. Hu *et al.*, ZipSeq: barcoding for real-time mapping of single cell transcriptomes. *Nat Methods* **17**, 833-843 (2020).
19. I. G. House *et al.*, Macrophage-Derived CXCL9 and CXCL10 Are Required for Antitumor Immune Responses Following Immune Checkpoint Blockade. *Clin Cancer Res* **26**, 487-504 (2020).
20. J. P. Bottcher *et al.*, NK Cells Stimulate Recruitment of cDC1 into the Tumor Microenvironment Promoting Cancer Immune Control. *Cell* **172**, 1022-1037 e1014 (2018).

21. A. Ray *et al.*, Multimodal identification of rare potent effector CD8 T cells in solid tumors. *Biorxiv*, (2023).
22. A. J. Combes *et al.*, Discovering dominant tumor immune archetypes in a pan-cancer census. *Cell* **185**, 184-203.e119 (2022).
23. V. Kumar *et al.*, Cancer-Associated Fibroblasts Neutralize the Anti-tumor Effect of CSF1 Receptor Blockade by Inducing PMN-MDSC Infiltration of Tumors. *Cancer Cell* **32**, 654-668 e655 (2017).
24. S. A. O'Brien *et al.*, Activity of tumor-associated macrophage depletion by CSF1R blockade is highly dependent on the tumor model and timing of treatment. *Cancer Immunol Immunother* **70**, 2401-2410 (2021).
25. C. H. Ries *et al.*, Targeting tumor-associated macrophages with anti-CSF-1R antibody reveals a strategy for cancer therapy. *Cancer Cell* **25**, 846-859 (2014).
26. S. Naik *et al.*, Commensal-dendritic-cell interaction specifies a unique protective skin immune signature. *Nature* **520**, 104-108 (2015).
27. M. Greter *et al.*, GM-CSF controls nonlymphoid tissue dendritic cell homeostasis but is dispensable for the differentiation of inflammatory dendritic cells. *Immunity* **36**, 1031-1046 (2012).
28. A. Swierczak *et al.*, The promotion of breast cancer metastasis caused by inhibition of CSF-1R/CSF-1 signaling is blocked by targeting the G-CSF receptor. *Cancer Immunol Res* **2**, 765-776 (2014).
29. S. Culemann *et al.*, Stunning of neutrophils accounts for the anti-inflammatory effects of clodronate liposomes. *J Exp Med* **220**, (2023).
30. C. A. Gomez-Roca *et al.*, Phase I study of emactuzumab single agent or in combination with paclitaxel in patients with advanced/metastatic solid tumors reveals depletion of immunosuppressive M2-like macrophages. *Ann Oncol* **30**, 1381-1392 (2019).
31. V. Juric *et al.*, TREM1 activation of myeloid cells promotes antitumor immunity. *Sci Transl Med* **15**, eadd9990 (2023).
32. M. K. Ruhland *et al.*, Visualizing Synaptic Transfer of Tumor Antigens among Dendritic Cells. *Cancer Cell* **37**, 786-799.e785 (2020).
33. K. Kersten *et al.*, Spatiotemporal co-dependency between macrophages and exhausted CD8. *Cancer Cell* **40**, 624-638.e629 (2022).
34. J. J. Engelhardt *et al.*, Marginating dendritic cells of the tumor microenvironment cross-present tumor antigens and stably engage tumor-specific T cells. *Cancer Cell* **21**, 402-417 (2012).
35. I. Korsunsky *et al.*, Fast, sensitive and accurate integration of single-cell data with Harmony. *Nat Methods* **16**, 1289-1296 (2019).
36. A. Dobin *et al.*, STAR: ultrafast universal RNA-seq aligner. *Bioinformatics* **29**, 15-21 (2013).
37. B. Li, C. N. Dewey, RSEM: accurate transcript quantification from RNA-Seq data with or without a reference genome. *BMC Bioinformatics* **12**, 323 (2011).

Acknowledgments:

Funding:

National Institutes of Health Grants: NIH R01CA197363 and NIH R37AI052116

AR was supported by a Cancer Research Institute Postdoctoral Fellowship (CRI2940)

KHH was supported by an American Cancer Society and Jean Perkins Foundation Postdoctoral Fellowship

NFK was supported by the Cancer Research Institute / Merck Postdoctoral Fellowship (CRI4546)

We thank members of the Krummel lab for their inputs to the manuscript.

Author Contributions:

Conceptualization: AR, MFK

Experimentation: AR, KK, NFK

ZipSeq: KHH, AR

Human tumor data curation: AJC, BS

Writing: AR, MFK

Supervision: MFK

Declaration of Interests:

The authors declare no competing interests

Data and materials availability:

Relevant data will be made publicly available before publication in its final form. Meanwhile, data will be available upon reasonable request, please contact the authors directly.

List of Supplementary Materials:

Materials and Methods

Fig. S1-S8

Figure and Figure Legends:

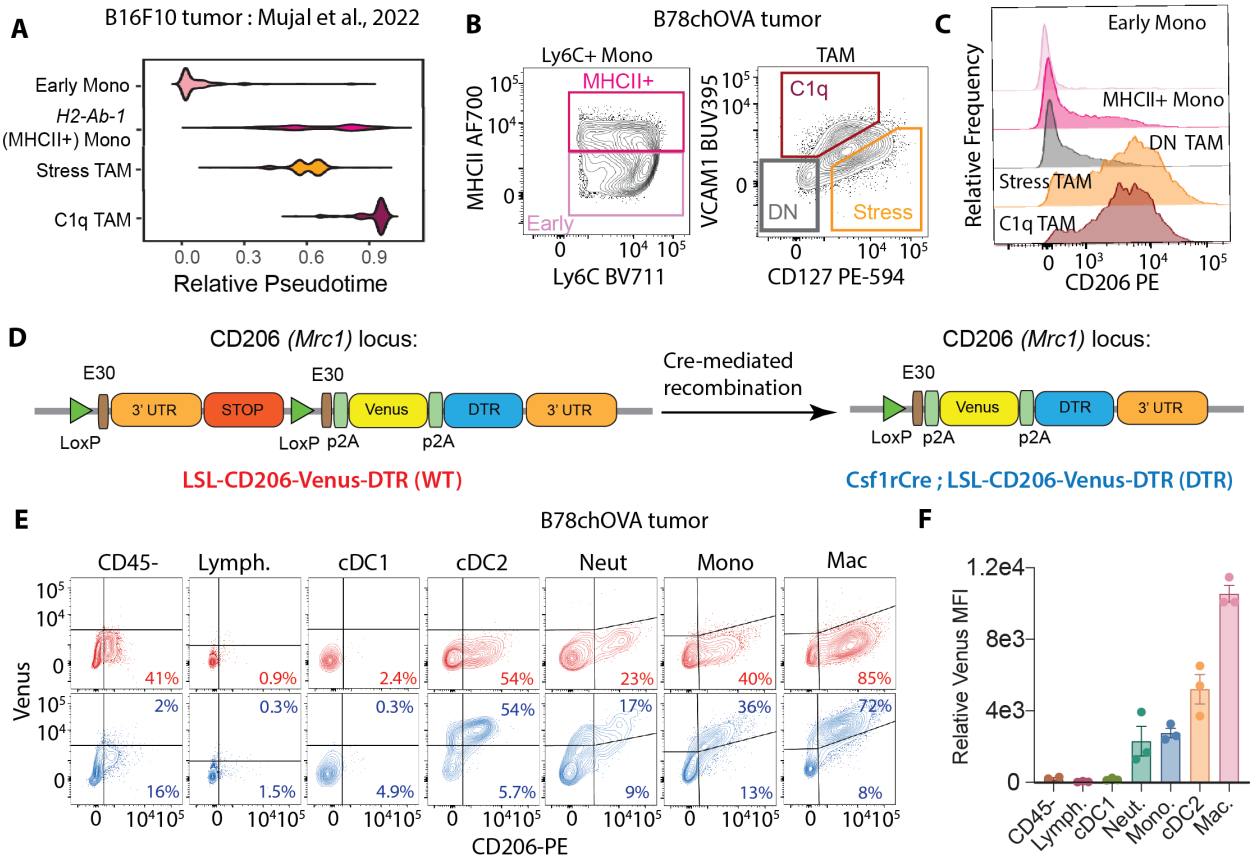

Fig. 1: A novel mouse model to mark and deplete CD206+ macrophages in tumors: (A) Pseudotime plots of select Monomac subsets in B16F10 tumors from Mujal et al(*3*); **(B)** Gating on the equivalent subsets in B78chOVA tumors by flow cytometry and **(C)** CD206 expression in each of these subsets; **(D)** Schematic representation of the *Mrc1*$^{\text{LSL-Venus-DTR}}$ knock-in construct before (WT) and after (DTR) Cre-mediated recombination by crossing to the *Csf1r*$^{\text{Cre}}$ allele; **(E)** Flow cytometry plots showing reporter (Venus, and therefore, DTR) and CD206 expression in different immune cells in d18 B78chOVA tumors in WT (red) and DTR (blue) mice with **(F)** quantification of relative reporter expression (DTR – WT) in the different subsets. data are mean +/- SEM, from 3 biological replicates, WT levels averaged from 2 biological duplicates.

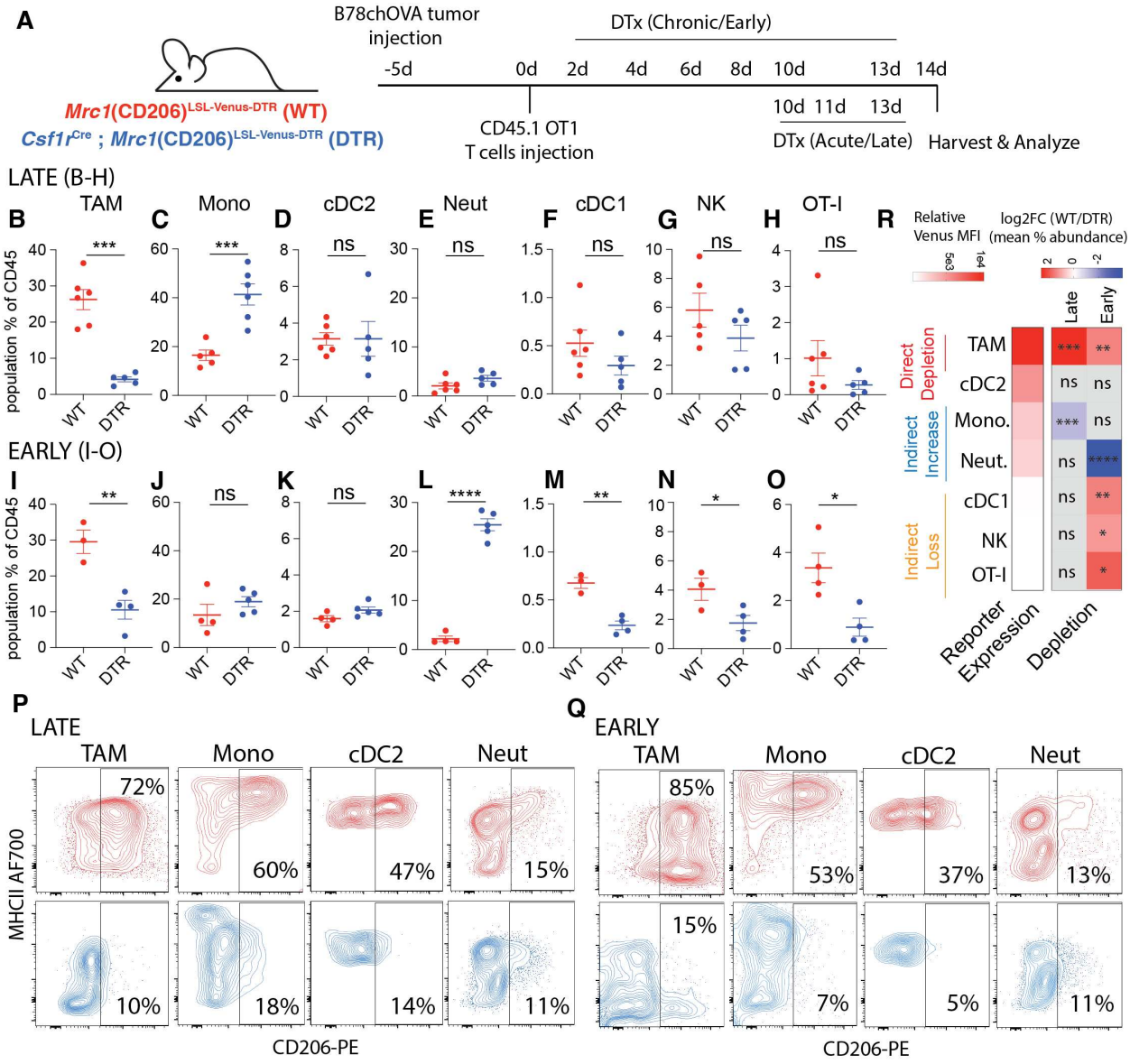

Fig. 2: Early CD206+ TAM depletion leads to a coordinated and indirect loss of NK:cDC1:CD8 cells in this TME: (A) Schematic representation of the experimental setup for early and late CD206+ TAM depletion in B78chOVA tumors using *Mrc1*(CD206)$^{LSL\text{-}Venus\text{-}DTR}$ (WT) and *Csf1r*^{Cre}; CD206$^{LSL\text{-}Venus\text{-}DTR}$ (DTR) mice; Relative abundance of different immune populations as a percentage of CD45+ cells with **(B-H)** late and **(I-O)** early depletion regimens; Representative flow cytometry plots showing CD206 vs. MHCII expression in different myeloid subsets in WT (red) and DTR (blue) mice in the (**P**) late and (**Q**) early depletion regimens. **(R)** heatmap representation of the log fold change of the ratio of mean abundances in WT and DTR mice (data from B-O), alongside the extent of reporter expression (mean relative Venus MFI from Fig. 1F) to indicate direct depletion and indirect loss or enrichment. (statistical significance is indicated on the respective squares; ***p <0.001, **p<0.01, *p <0.05, ns = no significance by Student's t-tests).

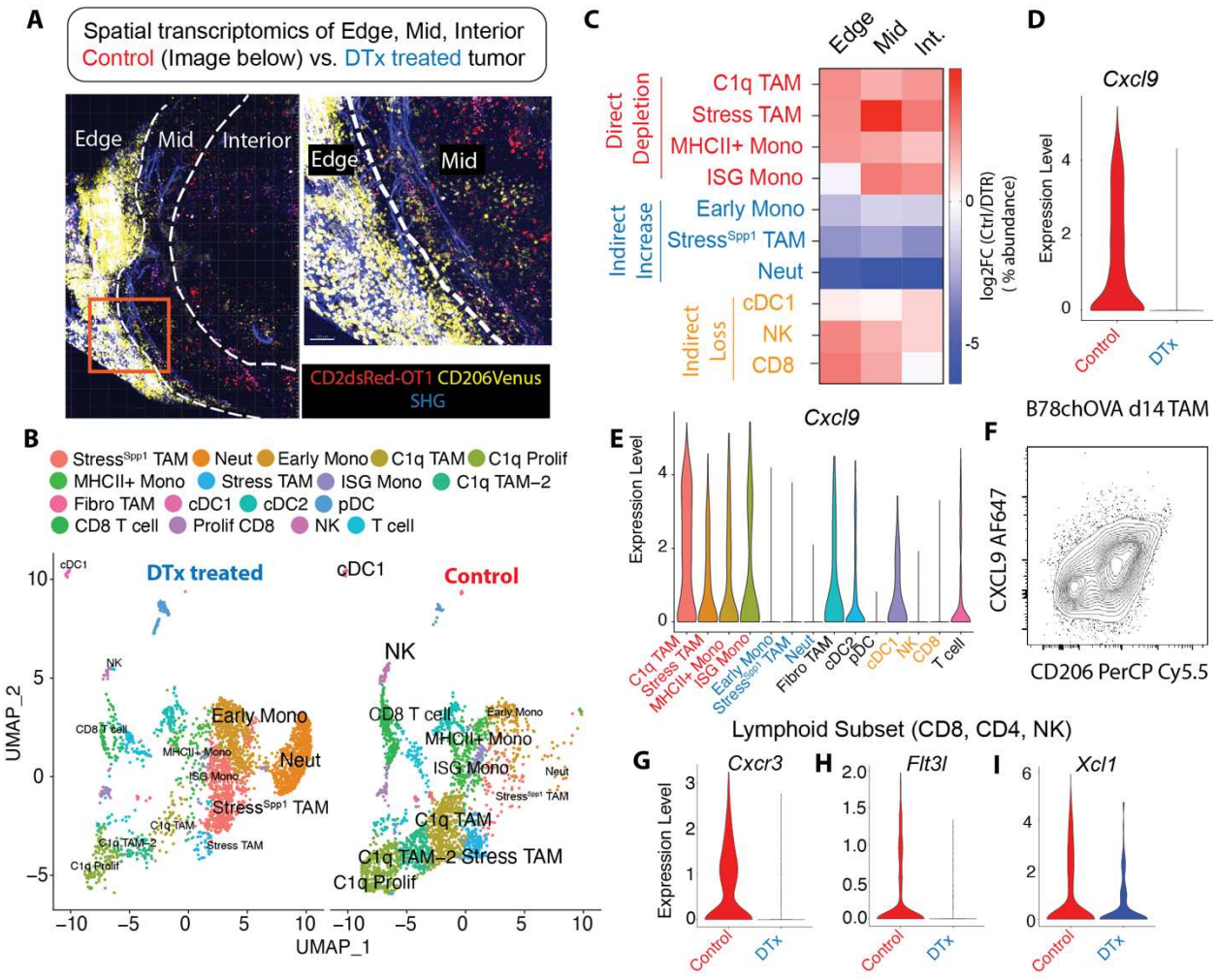

Fig. 3: CD206+ TAMs are enriched in production of CXCL9 and their loss leads to a decrease of *Cxcr3* positive lymphocytes: (A) Two-photon imaging of representative (control) B78chOVA tumors d12 post adoptive transfer of CD2dsRed; OT-I CD8 T cells showing three zones of Venus-expressing macrophage and associated CD8 T cell localization – edge, mid and interior (Int.) mapped by spatial transcriptomic barcoding ZipSeq; Boxed region is magnified (*right*) to show corresponding edge-mid interface SHG: Second Harmonic Generation; **(B)** UMAP representation of major immune cell populations obtained from Control and DTx treated B78chOVA tumors d12 post OT-I injection aggregated across all three regions; **(C)** Summary heatmap showing relative log fold change of the abundance (calculated as the % of the total number of cells recovered within that region) of each major cluster in Ctrl/DTx treated conditions, split by region of tumor; *Cxcl9* expression **(D)** aggregated across all clusters by treatment condition and **(E)** aggregated across treatment conditions by cluster; **(F)** Representative flow cytometry plot showing intracellular CXCL9 vs. surface CD206 expression in TAMs fraction in B78chOVA tumors at d14 post T cell adoptive transfer **(G)** *Cxcr3,* **(H)** *Flt3l* and **(I)** *Xcl1* expression in the lymphocyte subset (CD8 T cell, NK cell and CD4 T cell) by treatment group.

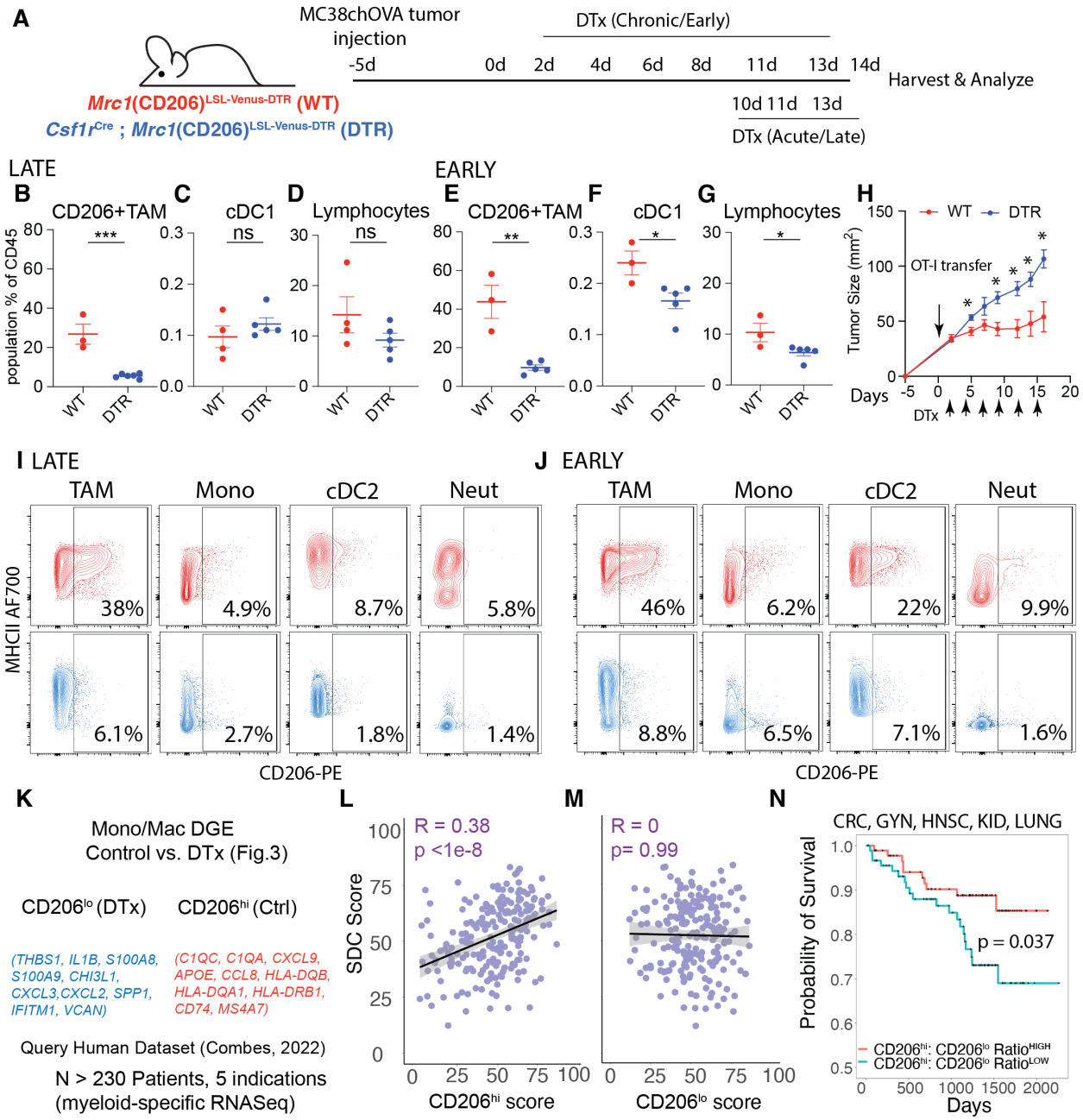

Fig. 4: CD206+ TAMs are important for anti-tumor immunity in mice and humans: (A) Schematic representation of the experimental setup for early and late CD206+ TAM depletion in MC38chOVA tumors using *Csf1r*^{Cre}; *Mrc1*$^{LSL\text{-}Venus\text{-}DTR}$ mice; Relative abundance of **(B, E)** CD206+ TAMs, **(C, F)** cDC1s and **(D, G)** lymphocytesas a percentage of CD45+ cells with late and early depletion regimens respectively; **(H)** tumor growth kinetics of MC38chOVA tumors in WT and DTR mice with DTx treatment beginning 2d post OT-I adoptive transfer at Day 0; Representative flow cytometry plots showing CD206 vs. MHCII expression in different myeloid subsets in WT (red) and DTR (blue) mice in the (**I**) late and (**J**) early depletion regimens; **(K)** Differential Gene Expression (DGE) of Monocytes and Macrophages (MonoMacs) in the Ctrl vs. DTx treated conditions (Fig. 3) showing the top 10 genes whose human orthologs were used to generate CD206^{hi} and CD206^{lo} MonoMac signature scores respectively to query the human dataset with

sorted myeloid bulk RNASeq data; The **(L)** $CD206^{hi}$, but not the **(M)** $CD206^{lo}$ MonoMac score correlated significantly with the stimulatory dendritic cell (SDC) score (Pearson R and p value for the null hypothesis that there is not a correlation are noted) and **(N)** the ratio of the $CD206^{hi}$:$CD206^{lo}$ score was a prognostic for increased survival of patients in a combined cohort including 5 major indications (CRC, GYN, LUNG, KID, HNSC) in the dataset – the cohort split into top and bottom 40% of the aforementioned ratio in the analysis shown, p value for the log-rank test is noted, ***p <0.001, **p<0.01, *p <0.05, ns = no significance by Student's t-tests.

Supplementary Materials for

Critical role of CD206+ macrophages in organizing anti-tumor immunity

Arja Ray[1,2], Kenneth H. Hu[1,2,#], Kelly Kersten[1,2], Nicholas F. Kuhn[1,2], Bushra Samad[2,3], Alexis J. Combes[1,2,3,4], Matthew F. Krummel[1,2,3*]

Affiliations:
[1]Department of Pathology, [2]ImmunoX Initiative, [3]UCSF CoLabs, [4]Department of Medicine, University of California, San Francisco, CA 94143, USA. [#]Current Address: Department of Immunology, The University of Texas MD Anderson Cancer Center and James P Allison Institute

***Corresponding Author:**
Matthew F. Krummel, Ph.D.
513 Parnassus Avenue, HSW 512
San Francisco, CA 94143-0511
matthew.krummel@ucsf.edu
Tel: (415) 514-3130
Fax: (415) 514-3165

Materials and Methods:

Mice: All mice were treated in accordance with the regulatory standards of the National Institutes of Health and American Association of Laboratory Animal Care and were approved by the UCSF Institution of Animal Care and Use Committee. *Mrc1*(CD206)$^{LSL\text{-}Venus\text{-}DTR}$ mice in the C57BL6/J background were custom-generated from Biocytogen Inc. and then maintained heterozygous (bred to C57BL6/J wild type mice) at the UCSF Animal Barrier facility under specific pathogen-free conditions. C57BL6/J (wild type; WT), C57BL6/J CD45.1 (B6.SJL-Ptprc^{a} Pepc^{b}/BoyJ), OT-I (C57BL/6-Tg(TcraTcrb)1100Mjb/J), Csf1r^{Cre} (C57BL/6-Tg(Csf1r-cre)1Mnz/J) mice were purchased for use from Jackson Laboratories and maintained in the same facility in the C57BL6/J background. For adoptive transfer experiments, CD45.1^{het}; OT-I^{het} (denoted simply as CD45.1; OT1) mice were used. Mice of either sex ranging in age from 6 to 14 weeks were used for experimentation.

Diphtheria toxin administration: For depletion of CD206-expressing macrophages, 500ng (20ng/g body weight, assuming an average 25g weight for each mouse) diphtheria toxin (DTx; List Biological Laboratories) in 100µL 1X PBS was injected intraperitoneally into each mouse – for both *Csf1r*^{Cre}; *Mrc1*(CD206)$^{LSL\text{-}Venus\text{-}DTR}$ (DTR) and *Mrc1*(CD206)$^{LSL\text{-}Venus\text{-}DTR}$ (WT) groups - at every time point. For the early depletion regime, injections were started 2 days after adoptive transfer of T cells and continued every 2-3 days till endpoint, while for the late depletion regime, injections began at d10 after T cell injection and continued till endpoint. For testing the effects of DTx in tumor-free tissue, similar dosing of DTx as the early depletion regime was implemented without tumor injection, and the skin (ectopic tumor site) and skin-draining lymph nodes were isolated for analysis. Mice were found to be healthy and without frank health issues with 6 doses of 500ng DTx (early depletion regime), but were monitored nevertheless throughout the experiment, as per IACUC guidelines.

Mouse tumor digestion and flow cytometry: Tumors from mice were processed to generate single cell suspensions as described previously(*17*). Briefly, tumors were isolated and mechanically minced on ice using razor blades, followed by enzymatic digestion with 200 µg/mL DNAse (Sigma-Aldrich), 100U/mL Collagenase I (Worthington Biochemical) and 500U/mL Collagenase IV (Worthington Biochemical) for 30 min at 37°C while shaking. Digestion was quenched by adding excess 1X PBS, filtered through a 100µm mesh, spun down and red blood cells were removed by incubating with RBC lysis buffer (155 mM NH_4Cl, 12 mM $NaHCO_3$, 0.1 mM EDTA) at room temperature for 10 mins. The lysis was quenched with excess 1X PBS, spun down and resuspended in FACS buffer (2mM EDTA + 1% FCS in 1X PBS) to obtain single cell suspensions. Similarly, tumor draining lymph nodes (dLN) were isolated and mashed over 100µm filters in PBS to generate single cell suspensions.

For each sample, 2.5-3 million cells/sample were stained in a total of 50µL of antibody mixture for flow cytometry. Cells were washed with PBS prior to staining with Zombie NIR Fixable live/dead dye (1:500) (Biolegend) for 20 min at 4°C. Cells were washed in FACS buffer followed by surface staining for 30 min at 4°C with directly conjugated antibodies diluted in FACS buffer containing 1:100 anti-CD16/32 (Fc block; BioXCell) to block non-specific binding. Antibody dilutions ranged from 1:100-1:400, optimized separately. After surface staining, cells were washed again with FACS buffer. For intracellular staining, cells were fixed for 20 min at 4°C using the IC Fixation Buffer (BD Biosciences) and washed in permeabilization buffer from the FoxP3 Fix/Perm Kit (BD Biosciences). Antibodies against intracellular targets were diluted in permeabilization buffer containing 1:100 Fc Block and cells were incubated for 30 min at 4°C followed by another wash prior to readout on a BD LSRII or Fortessa Cytometer.

Processing and flow cytometry analysis of other mouse organs: To phenotype cells from lymphoid organs, spleen or inguinal, axillary and brachial (tumor-draining) lymph nodes were isolated, pried open with tweezers (lymph nodes) or cut into small pieces (spleen) and digested

with the same digestion cocktail as above, intermittently pipetting with cut P1000 pipette tips to enhance mechanical digestion. The resulting suspensions were then filtered using 100µm filter, washed with 1X PBS to generate single cell suspensions. For splenic digests, RBC lysis was performed as described above before staining for flow cytometry.

For lung digests both lobes were isolated, cut into small pieces with scissors and minced by using gentleMACS dissociator (Miltenyi Biotec) in RPMI. Next, the mixture was spun down and resuspended in the digestion mixture described above and allowed to digest with shaking at 37°C for 20 mins, following which, the remaining tissue was either minced again using the gentleMACS dissociator and/or directly mashed over a 100µm filter in FACS buffer to generate a single cell suspension, ready to be processed for staining and flow cytometry.

Skin digestion was done as previously described(*32*). Briefly, mice were shaved and depilated prior to removal of dorsal skin. The skin was then rid of fat, minced with scissors and razor blade in the presence of 1 ml of digest media (2 mg/ml collagenase IV (Roche), 1 mg/ml hyaluronidase (Worthington), 0.1 mg/ml DNase I (Roche) in RPMI-1640 (GIBCO). The minced skin was then moved to a 50 ml conical with 5 ml additional digest solution and incubated at 37°C for 45 min with shaking and intermittent vortexing before being washed and passed through a 70µm strainer prior to staining.

Flow cytometry Data Analysis: Analysis of flow cytometry data was done on FlowJo and later plotted on GraphPad Prism or R. Relative MFI of the Venus reporter was calculated by subtracting the background average MFI of the same channel in WT samples from those in each DTR sample. For analysis of a shift in relative abundance of a population x (Fig. 2), the $\log_2$ (% x of CD45 in WT/ % x of CD45 in DTR) was calculated and plotted as a heatmap, such that positive values indicate depletion and negative values indicate enrichment.

Tumor injections and adoptive transfer of CD8 T cells into tumors: The B78chOVA and MC38chOVA cancer cell lines, as previously described(*17, 33*), were generated by incorporating the same mcherry-OVA construct used to establish the PyMTchOVA spontaneous mouse line(*34*). For tumor injections, the corresponding cells were grown to near confluency (cultured in DMEM with 10% FCS (Benchmark) and 1% PSG (Gibco)) and harvested using 0.05% Trypsin-EDTA (Gibco) and washed 3x with PBS (Gibco). The number of cells to be injected per mouse was resuspended in PBS to a final volume of 50µL per injection. The suspension was injected subcutaneously into the flanks of anesthetized and shaved mice. Tumors were allowed to grow for 14–21 days unless otherwise noted, before tumors and tumor-draining lymph nodes were harvested for analysis. CD8 T cells were isolated from CD45.1;OT-1;Cd69-TFP mice using the EasySep Negative Selection Kit (Stem Cell Bio), resuspended in 1X PBS at 10X concentration 100µL was injected into each tumor-bearing mice. For B78chOVA 1 million and for MC38chOVA tumors, 200,000 CD8 T cells were injected retro-orbitally into each mouse either 5d (B78chOVA), 7d (MC38chOVA) post tumor injection. Tumor measurements were done by measuring the longest dimension (length) and approximately perpendicular dimension (width) using digital calipers, rounded to one decimal place each.

Spatial single cell RNA Sequencing and Analysis: Spatial scSeq of immune cell populations at the tumor edge, interface and interior zones was performed using ZipSeq, as previously described(*11*), with the additional condition of DTx treatment integrated into the dataset. Briefly, B78chOVA tumors subcutaneously grown in Csf1rCre; CD206$^{LSL\text{-}Venus\text{-}DTR}$ mice d12 post adoptive transfer of 1 million CD2dsRed; OT-I CD8 T cells with (DTx) and without (Control) DTx treatment (early depletion regime) were harvested and sliced into 160µm slices using a Compressotome (Precisionary Instruments VFZ-310-0Z). Imaging, spatial barcoding, subsequent digestion, sorting, encapsulation (10X Genomics) and library construction, CellRanger processing and alignment were performed as described previously(*11, 18*). The two separate sequencing runs

(Control and DTx) were assembled and integrated into a single data structure using Harmony(*35*). The final object underwent scaling and then scoring for cell cycle signatures (S and G2M scores as computed using Seurat's built-in CellCycleScoring function. The object then underwent regression for cell cycle effects (S and G2M score as described in the Seurat vignette) and percent mitochondrial reads before PCA.

Relative abundance from scSeq data was calculated by: log2 (% of each cluster (cell type) within a tumor region (Edge, Mid, Inner) in the Ctrl / (% of the same cluster in the same region in the DTx treated group), thereby yielding positive values for depletion and negative values for enrichment. While abundances were calculated with the broad clusters from the overall object, the lymphoid clusters were isolated to a separate object, re-clustered to further probe for individual gene expression (*Cxcr3, Flt3l, Xcl1*) in the resulting subsets.

Human tumor samples: All tumor samples were collected with patient consent after surgical resection under a UCSF IRB approved protocol (UCSF IRB# 20-31740), as described previously(*22*). In brief, freshly resected samples transported in ice-cold DPBS or Leibovitz's L-15 medium before digestion and processing to generate a single-cell suspension. The five most well-represented cancer indications in this collection were included in the cohort: Colorectal cancer (CRC), gynecological cancers (GYN), head and neck cancer (HNSC), kidney cancer (KID), lung cancer (LUNG). Clinical data including survival of patients were obtained through regular clinical follow-up at UCSF.

Transcriptomic analysis of human tumors: All tumor samples were collected under the UCSF Immunoprofiler project as described(*22*). Briefly, tumor samples were thoroughly minced with surgical scissors and transferred to GentleMACS Tubes containing 800 U/ml Collagenase IV and 0.1 mg/ml DNase I in L-15/2% FCS per 0.3 g tissue. GentleMACS Tubes were then installed onto

the GentleMACs Octo Dissociator (Miltenyi Biotec) and incubated for 20 min (lymph node) or 35 min (tumor) according to the manufacturer's instructions. Samples were then quenched with 15 mL of sort buffer (PBS/2% FCS/2mM EDTA), filtered through 100µm filters and spun down. Red blood cell lysis was performed with 175 mM ammonium chloride, if needed. Freshly digested tumor samples were sorted by FACS into conventional T cell, Treg, Myeloid, tumor and in some cases, stromal compartments and bulk RNA-seq was performed on sorted cell fractions. mRNA was isolated from sorted fractions and libraries were prepared using Illumina Nextera XT DNA Library Prep kit. The libraries were sequenced using 100bp paired end sequencing on HiSeq4000. The sequencing reads we aligned to the Ensembl GRCh38.85 transcriptome build using STAR(*36*) and gene expression was computed using RSEM(*37*). Sequencing quality was evaluated by in-house the EHK score, where each sample was assigned a score of 0 through 10 based on the number of EHK genes that were expressed above a precalculated minimum threshold. The threshold was learned from our data by examining the expression distributions of EHK genes and validated using the corresponding distributions in TCGA. A score of 10 represented the highest quality data where 10 out of 10 EHK genes are expressed above the minimum threshold. The samples used for survival analysis and other gene expression analyses had an EHK score of greater than 7 to ensure data quality. Ensemble gene signatures scores were calculated by converting the expression of each gene in the signature to a percentile rank among all genes and then determining the mean rank of all the genes in the signature (*21*). The corresponding gene list for obtaining the stimulatory dendritic cell score is as described before(*10*). For survival analysis, patients were split into ($CD206^{hi}$:$CD206^{lo}$ gene signature ratio)^{HIGH} (top 40%) vs. ($CD206^{hi}$:$CD206^{lo}$ gene signature ratio)^{LOW} (bottom 40%) and analyzed using a log-rank test.

679 **Two-photon imaging of tumor slices:** Tumor slices (adjacent to the ones used for spatial
680 barcoding by ZipSeq) were fixed in 2% paraformaldehyde (PFA; Sigma), washed and left
681 overnight in 1X PBS before imaging on a custom-made 2-photon microscope as previously
682 described(*10*) to visualize the Venus reporter and CD2dsRed marked CD8 T cells and fibrous
683 collagen by second harmonic generation (SHG). Dual laser excitations at 800nm and 950nm were
684 used to excite the requisite fluorophores.
685
686 **Statistical Analysis:** Statistical analysis was done in GraphPad Prism or in R. For testing null
687 hypothesis between two groups, either Student's t tests and or the non-parametric Mann-Whitney
688 U tests were used, depending on the number and distribution of data points. Likewise, for testing
689 null hypotheses among 3 or more groups, ANOVA or non-parametric tests were performed,
690 followed by post-hoc Holm-Sidak's test, correcting for multiple comparisons. Unless otherwise
691 mentioned, data are representative of at least 2 independent experiments.
692

Supplementary Figures and Figure Legends:

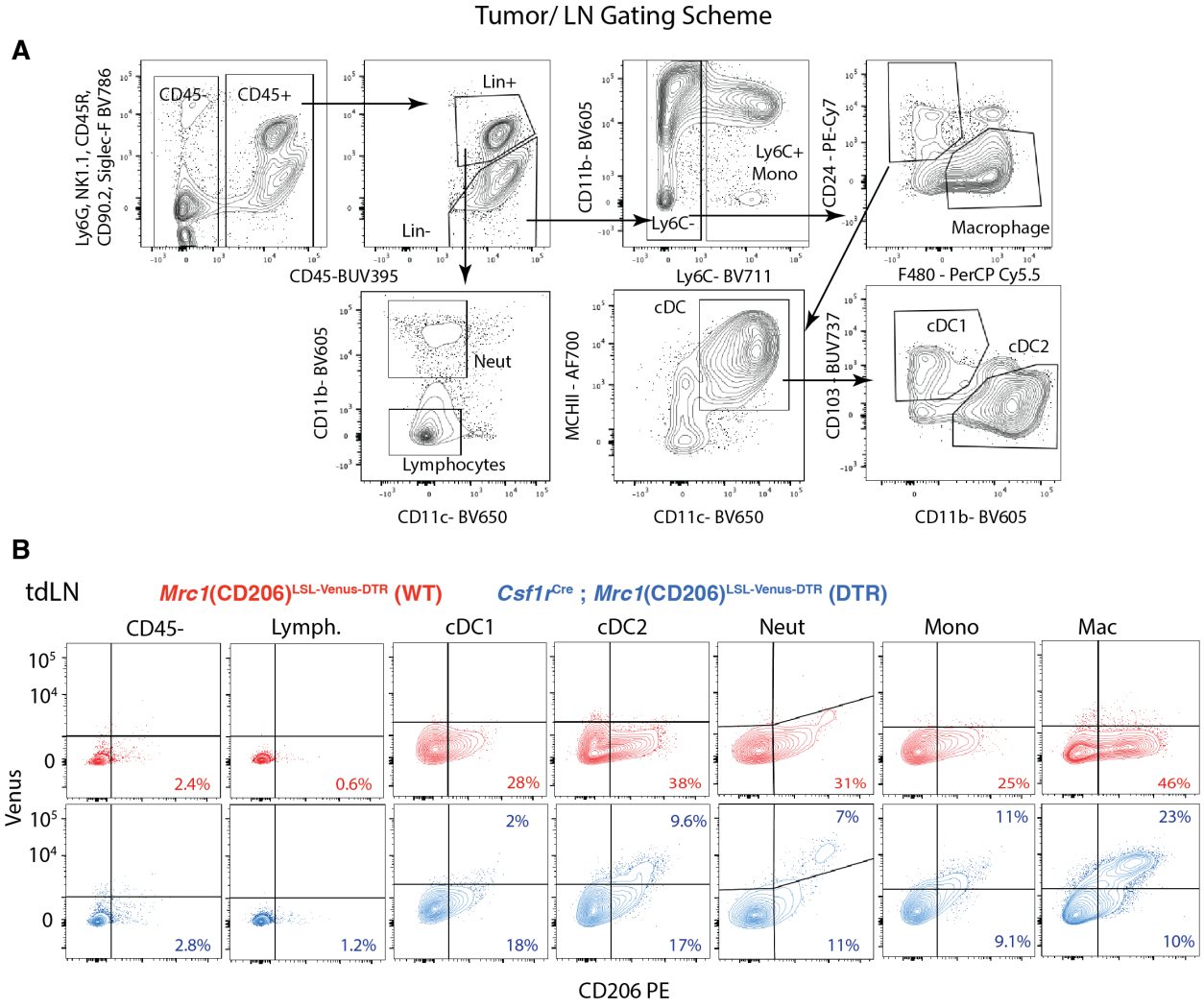

Fig. S1: CD206-Venus reporter expression in tdLN: (A) Representative flow cytometry gating scheme to identify myeloid cells and lymphocytes from tumor and tdLN; **(B)** Flow cytometry plots showing reporter (Venus, and therefore, DTR) and CD206 expression in different immune cells in d18 B78chOVA tdLN in WT (red; *Mrc1*$^{LSL\text{-}Venus\text{-}DTR}$) and DTR (blue; *Csf1r*^{Cre}; *Mrc1*$^{LSL\text{-}Venus\text{-}DTR}$) mice.

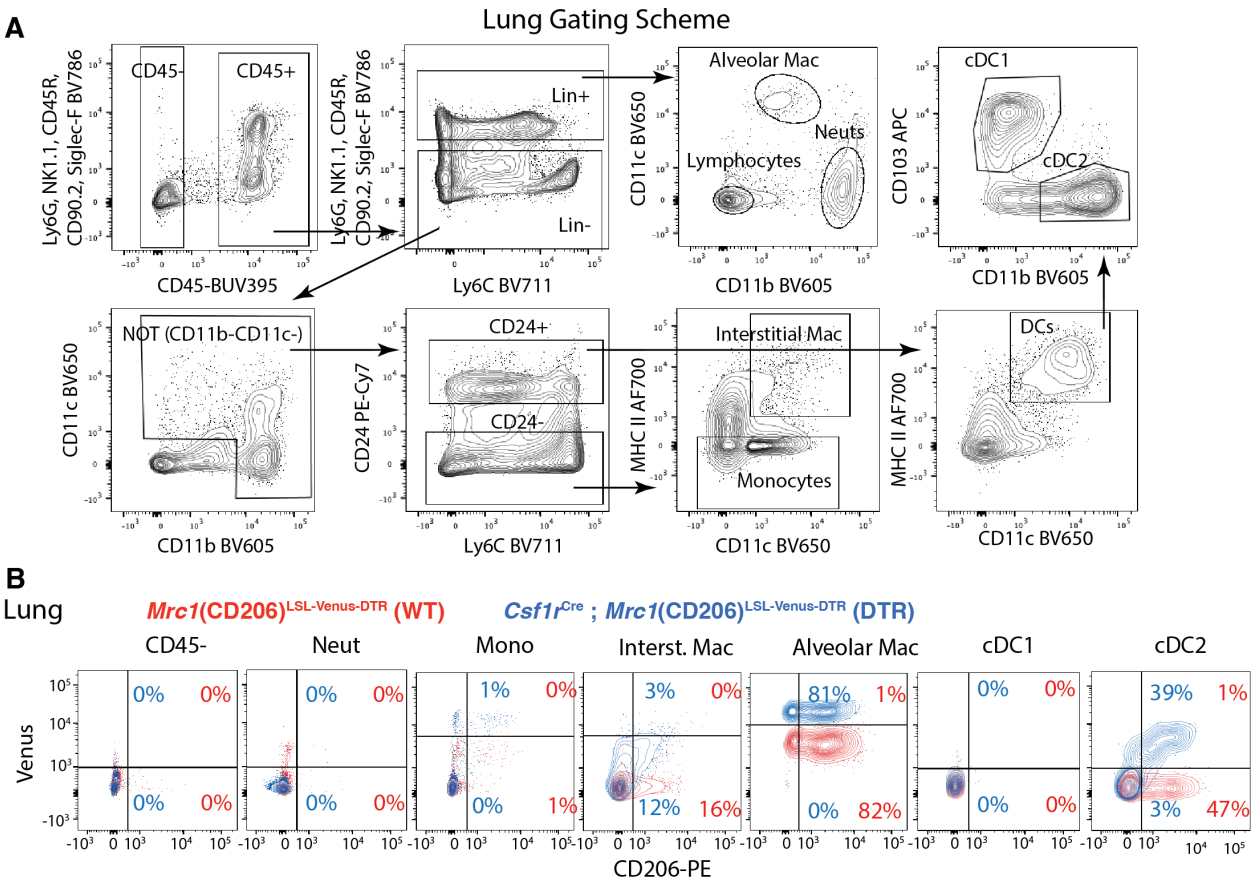

Fig. S2: CD206-Venus reporter expression in lungs: (A) Representative flow cytometry gating scheme to identify myeloid cells and lymphocytes from lungs; **(B)** Overlaid flow cytometry plots showing reporter (Venus, and therefore, DTR) and CD206 expression in different immune cells in lungs of WT (red; *Mrc1*$^{\text{LSL-Venus-DTR}}$) and DTR (blue; *Csf1r*$^{\text{Cre}}$; *Mrc1*$^{\text{LSL-Venus-DTR}}$) mice.

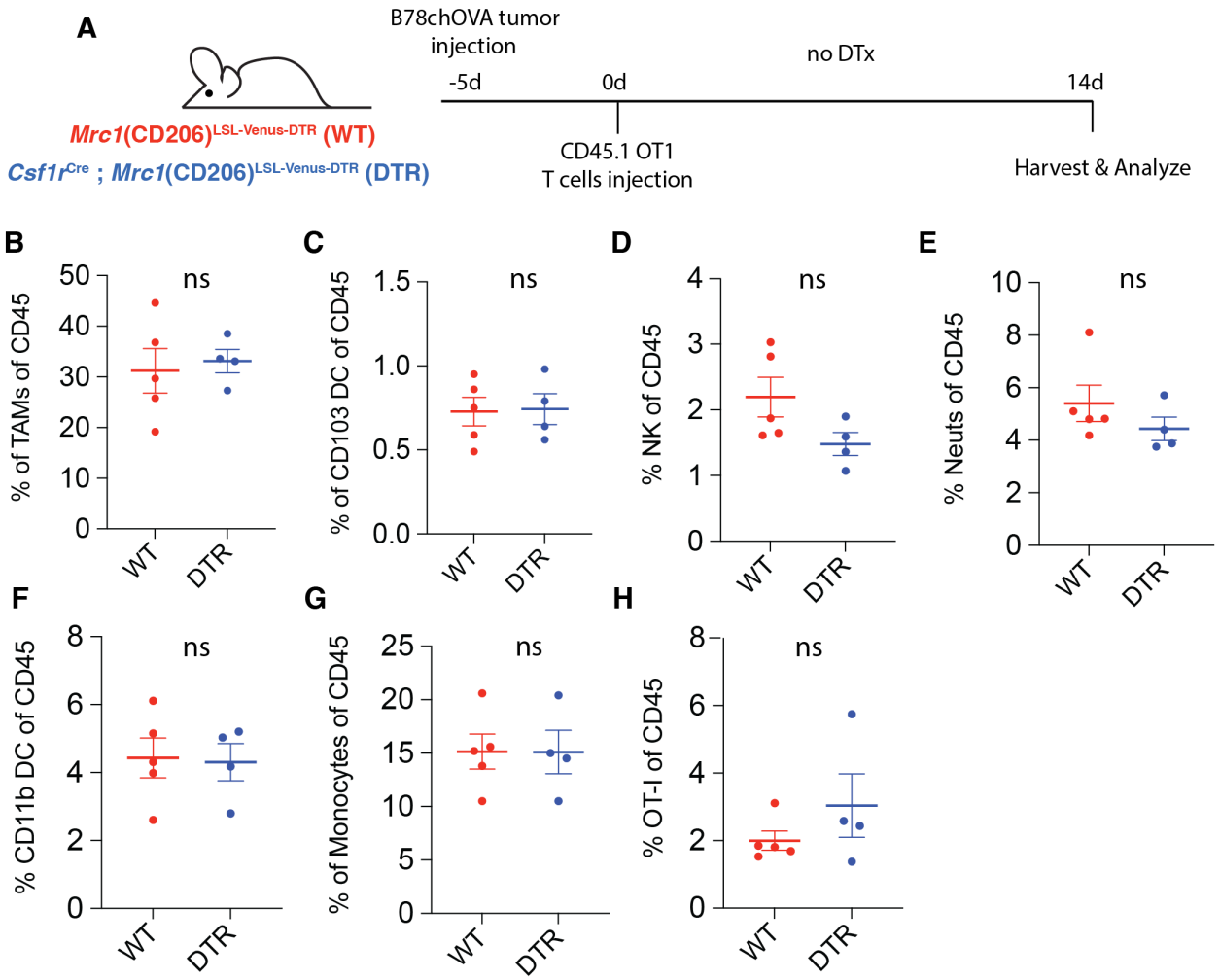

Fig. S3: Reporter expression in the absence of diptheria toxin does not alter immune composition in B78chOVA tumors (A) Schematic representation of the experimental setup for tumor injection, OT-I T cell adoptive transfer and analysis in CD206$^{LSL\text{-}Venus\text{-}DTR}$ (WT) and Csf1rCre; CD206$^{LSL\text{-}Venus\text{-}DTR}$ (DTR) mice; **(B-H)** Relative abundance of different immune populations as a percentage of CD45+ cells in the two groups of mice. ns = no significance by Student's t-tests.

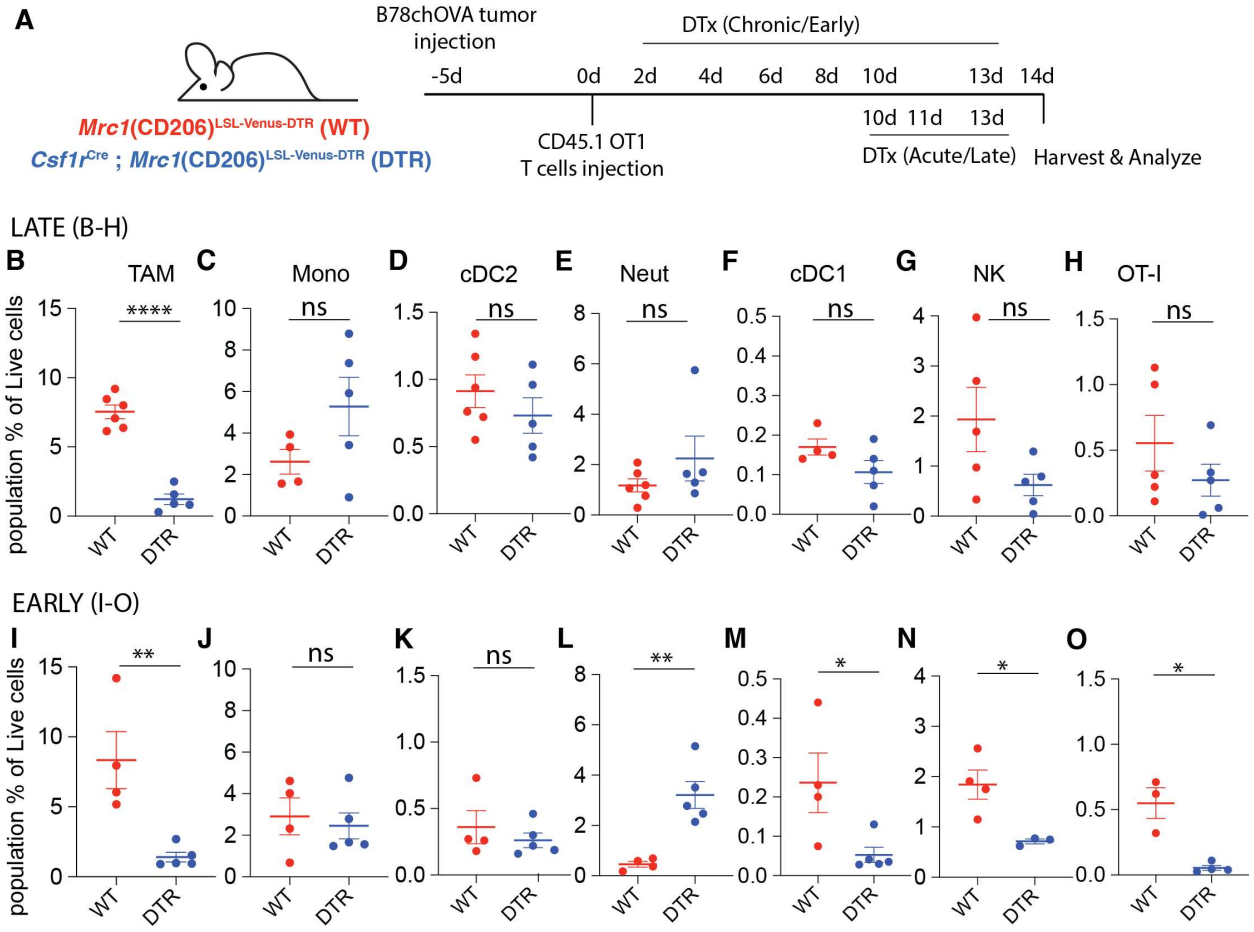

Fig. S4: Relative cell abundances as a percentage of total live compartment : (A) Schematic representation of the experimental setup for early and late CD206+ TAM depletion in B78chOVA tumors using *Mrc1*$^{\text{LSL-Venus-DTR}}$ (WT) and *Csf1r*$^{\text{Cre}}$; *Mrc1*$^{\text{LSL-Venus-DTR}}$ (DTR) mice; Relative abundance of different immune populations as a percentage of CD45+ cells with **(B-H)** late and **(I-O)** early depletion regimens. ****p<0.0001, **p<0.01, *p <0.05, ns = no significance by Student's t-tests.

728

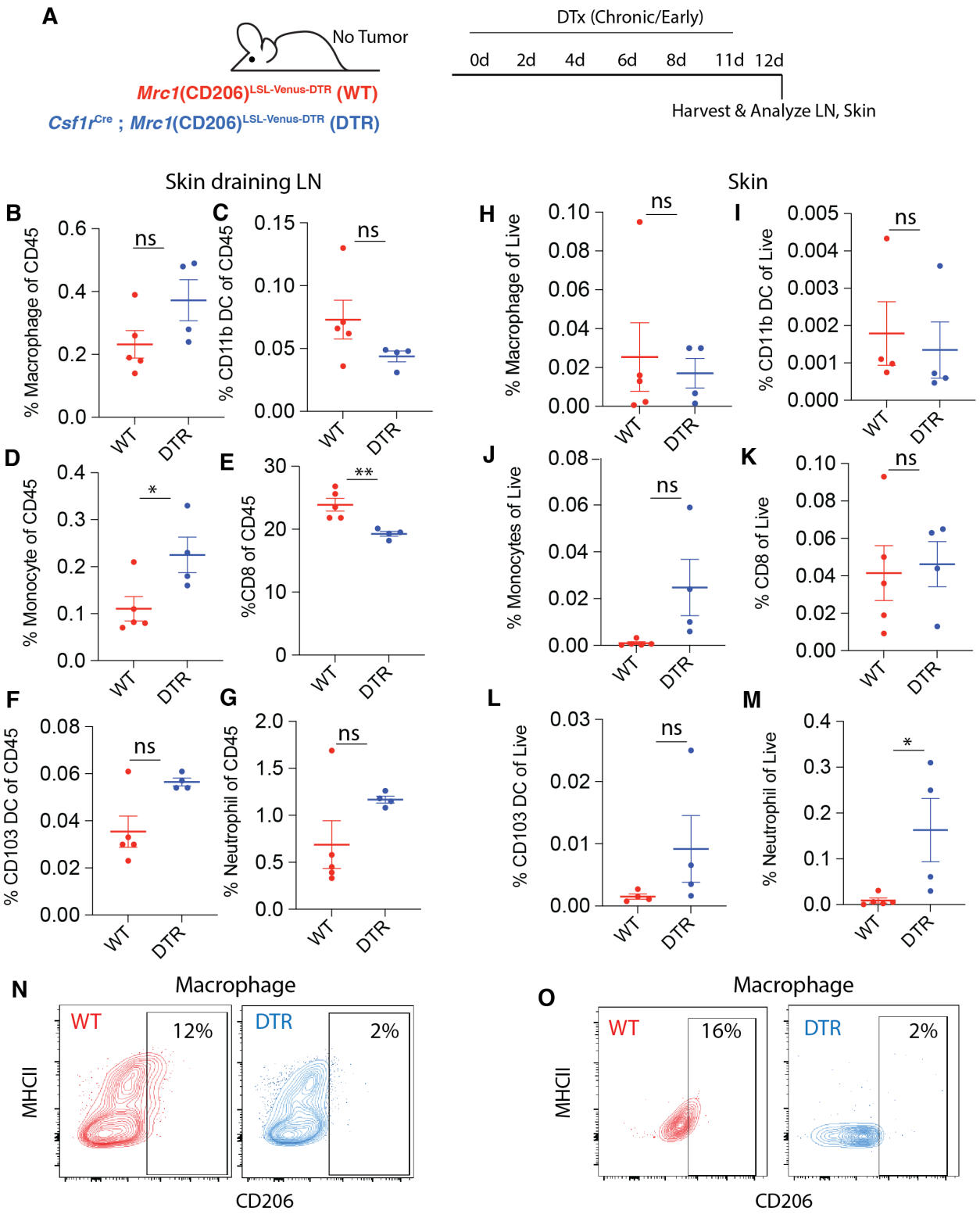

729
730
731 **Fig. S5: Chronic DTx treatment does not produce indirect cDC1 depletion in skin and skin-**
732 **draining LN: (A)** Schematic representation of the experimental setup for analysis of skin and
733 skin-draining LNs in *Mrc1*$^{\text{LSL-Venus-DTR}}$ (WT; red) and *Csf1r*$^{\text{Cre}}$; *Mrc1*$^{\text{LSL-Venus-DTR}}$ (DTR; blue) mice

734 with DTx administration; Relative abundance of different immune populations in the **(B-G)** skin-
735 draining LN and **(H-M)** skin as a percentage of CD45+ cells in the two groups of mice;
736 Representative flow cytometry plots showing CD206 and MHCII expression in the macrophages
737 of the two groups in **(N)** skin-draining LN and **(O)** skin. **p<0.01, *p <0.05, ns = no significance
738 by Student's t-tests.
739

740

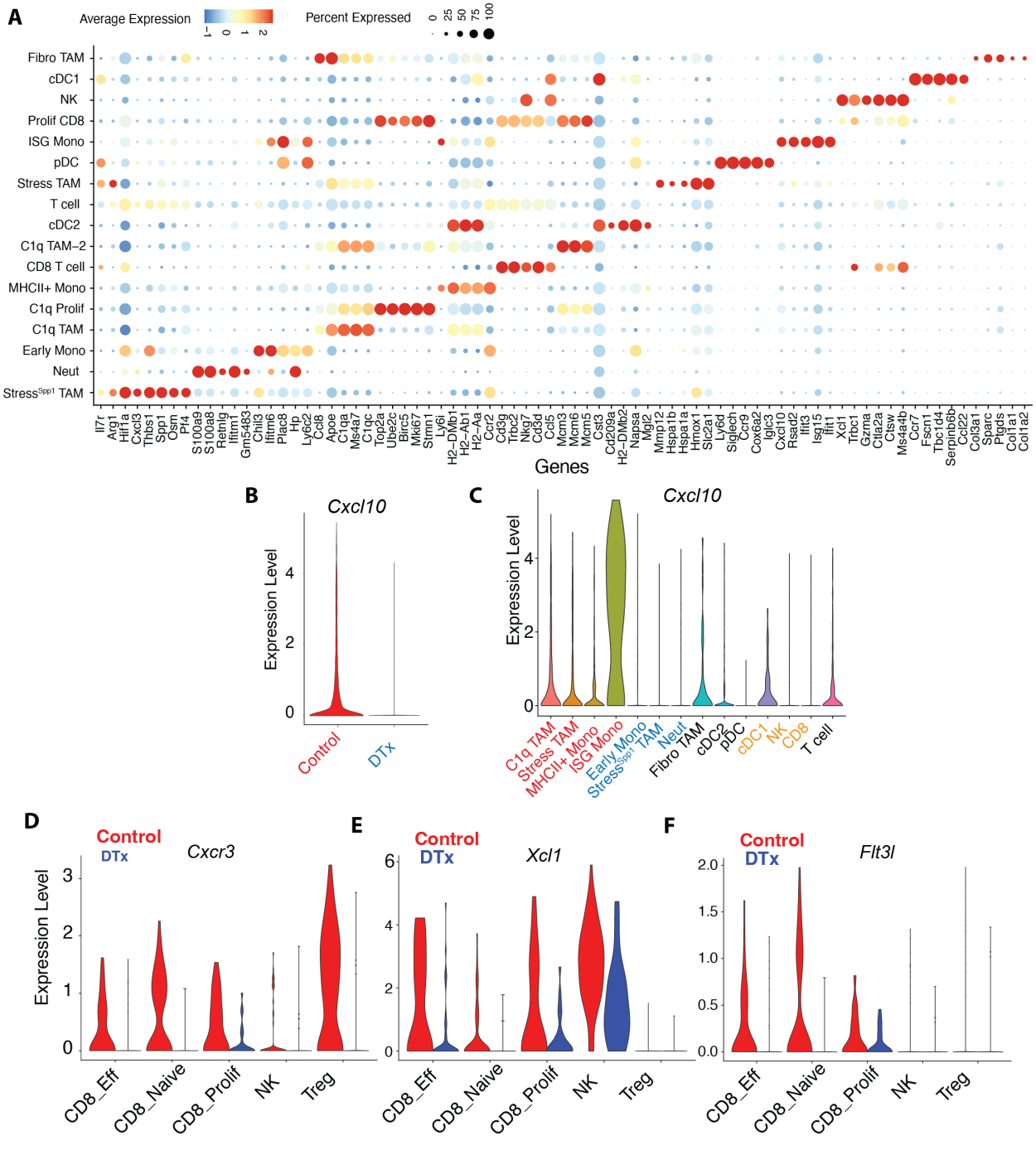

741
742

Fig. S6: CXCL9:CXCR3 axis is disrupted by depletion of CD206+ TAMs: (A) Dotplot representing top5 differentially expressed genes and select other genes in each immune cell cluster identified from a harmonized dataset of spatially barcoded Control and DTx treated B78chOVA tumors d12 post adoptive transfer of CD2dsRed; OT-I cells; *Cxcl10* expression **(B)** aggregated across all clusters by treatment condition and **(C)** aggregated across treatment conditions by cluster; Violin plot representing **(D)** *Cxcr3*, **(E)** *Xcl1* and **(F)** *Flt3l* expression in the lymphoid compartment in Control and DTx treated conditions.

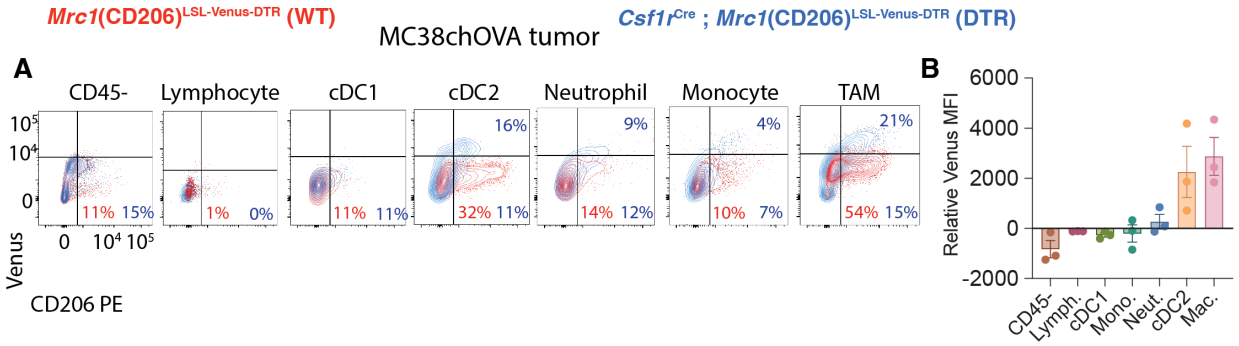

Fig. S7: CD206-Venus reporter expression in MC38chOVA tumors: (A) Overlaid flow cytometry plots showing reporter (Venus, and therefore, DTR) and CD206 expression in different immune cells in MC38chOVA tumors in WT (red; *Mrc1*$^{LSL\text{-}Venus\text{-}DTR}$) and DTR (blue; *Csf1r*^{Cre}; *Mrc1*$^{LSL\text{-}Venus\text{-}DTR}$) mice and **(B)** quantification of relative reporter expression (DTR – WT) in the different subsets. data are mean +/- SEM, from 3 biological replicates, WT levels averaged from 2 biological duplicates.

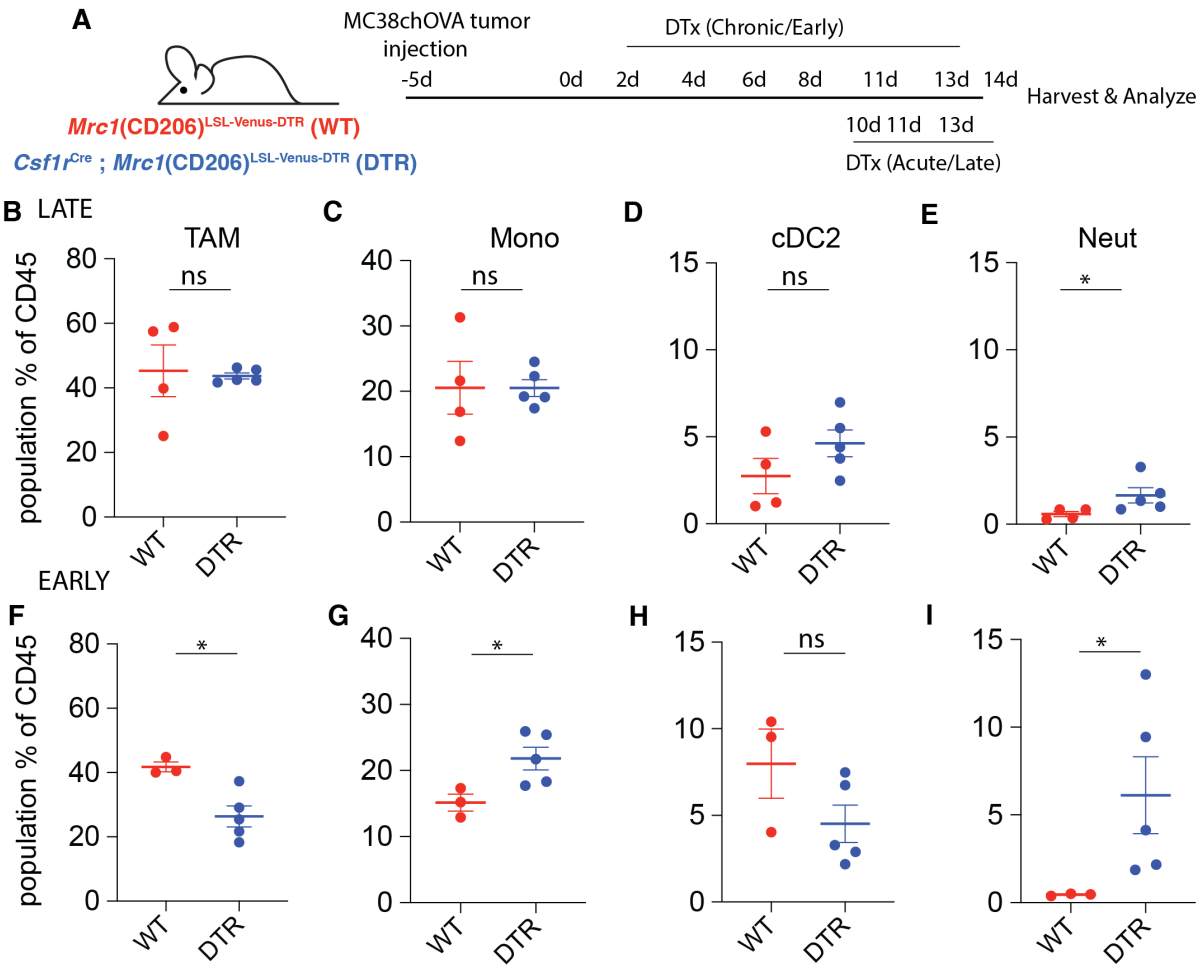

Fig. S8: Effect of CD206+ MonoMac depletion on MC38chOVA immune composition: (A) Schematic representation of the experimental setup for early and late CD206+ TAM depletion in MC38chOVA tumors using *Mrc1*$^{LSL\text{-}Venus\text{-}DTR}$ (WT) and *Csf1r*^{Cre}; *Mrc1*$^{LSL\text{-}Venus\text{-}DTR}$ (DTR) mice; Relative abundance of different immune populations as a percentage of CD45+ cells with **(B-E)** late and **(F-I)** early depletion regimes. data are mean +/- SEM, *p <0.05, ns = no significance by Student's t-tests.